Physics of Plasmas ARTICLE scitation.org/journal/php

Viscous dissipation in two-dimensional compression of turbulence

Cite as: Phys. Plasmas **26**, 082702 (2019); doi: 10.1063/1.5111961
Submitted: 31 May 2019 · Accepted: 15 July 2019 ·
Published Online: 7 August 2019

Seth Davidovits and Nathaniel J. Fisch

AFFILIATIONS

Department of Astrophysical Sciences, Princeton University, Princeton, New Jersey 08544, USA

ABSTRACT

Nonradial hydrodynamic flow can be generated or amplified during plasma compression by various mechanisms, including the compression itself. In certain circumstances, the plasma may reach a viscous state; for example, in compression experiments seeking fusion, the fuel plasma may reach a viscous state late in the compression due in part to the rising fuel temperature. Here, we consider viscous dissipation of nonradial flow in the case of initially isotropic, three-dimensional (3D), turbulent flow fields compressed at constant velocity in two dimensions. Prior work in the case of 3D compressions has shown the possibility of effective viscous dissipation of nonradial flow under compression. We show that, theoretically, complete viscous dissipation of the nonradial flow should still occur in the 2D case when the plasma heating is adiabatic and the viscosity has the (strong) Braginskii temperature dependence ($\mu \sim T^{5/2}$). However, in the general case, the amount of compression required is very large even for modest initial Reynolds numbers, with the compression reaching an intermediate state dominated by variations only in the noncompressed direction. We show that both the nonlinearity and boundary conditions can play important roles in setting the characteristics and ease of the viscous dissipation.

I. INTRODUCTION

Compression experiments seeking fusion of hydrogen fuel are carried out in both three-dimensions (typically with compression in the spherical radius) and two-dimensions (typically with compression in the cylindrical radius). Examples of the former are ignition experiments at the National Ignition Facility (NIF),[1,2] while examples of the latter are Magnetized Liner Inertial Fusion (MagLIF) experiments.[3,4] Detailed simulations seeking to understand the hydrodynamics of NIF ignition experiments have shown that flows in the fuel plasma, which can be generated by a variety of mechanisms during the compression, can be substantially affected by viscosity when the fuel becomes hot near bang time.[5,6] Viscous effects on nonradial flow in compressions (flow not associated with the compression itself) have also been studied in detail in isolation for the case of such 3D compressions.[7–14]

Nonradial flow in the fusion fuel can have a variety of impacts. At the most basic level, such motion can be regarded as "wasted" compression energy, if it remains as flow in the stagnation process and therefore is energy that is not converted to the high temperatures required for fusion. Even if this impact is negligible, small quantities of nonradial flow may degrade implosion performance,[15–18] for example, by causing mixing of the nonfuel capsule material, or cold fuel, into the hot-spot. As such, understanding the behavior of such flows is important, including the impacts that the viscosity has, if it grows large enough to influence the flow.

Here, we study the impact of a transition from inviscid to viscous on nonradial flows in 2D compressions. While this work has potential applications in understanding nonradial flow dynamics in 2D fusion compression experiments, we note that there is no magnetic field included in the present work, an important limitation to relax in future work. The present study is also useful to assess the possibility of utilizing sudden viscous dissipation[7] to achieve a new design for generating fusion or X-ray bursts in a 2D compression geometry, rather than the previously studied 3D compressions.

The rest of this paper is organized as follows: in Sec. II, we describe the set of equations used to model the 2D compression of 3D turbulence in this work. Then, in Sec. III, we calculate a linear solution to the 2D compression system, which is useful for understanding some key features of the viscous dissipation process. Section IV discusses the insights that can be gained from the linear solution and analyzes the results of (nonlinear) simulations of the full 2D compressing system. Finally, in Sec. V, we summarize the main results and discuss them in the context of sudden viscous dissipation and inertial fusion experiments.

II. APPROACH

In order to investigate the viscous dissipation process for 2D compressions, we use a plasma treatment similar to that in prior work on viscous dissipation in 3D.[7–9] See, in particular, the appendix in

Davidovits and Fisch.[8] As before, we consider the plasma behavior to be governed by the Navier-Stokes (NS) equations and assume the compression is caused by a given background flowfield, $v_{i0}(\mathbf{x},t) = A_{ij}(t)x_j$. The full flow in the NS momentum equation is $v_i(\mathbf{x},t) = v_{i0}(\mathbf{x},t) + v_i'(\mathbf{x},t)$, and our interest is to solve the behavior of the flow $v_i'(\mathbf{x},t)$, given the background flow. While, for the 3D case, we took an isotropic compression, $A_{ij}(t) = a(t)\delta_{ij}$, with δ_{ij} being the Kronecker delta, here we consider a 2D compression,

$$A_{ij}(t) = \begin{cases} a(t) & i = j = 1 \text{ or } i = j = 2 \\ 0 & \text{otherwise.} \end{cases} \tag{1}$$

As in the 3D case, we will have

$$a(t) = \frac{\dot{L}}{L}, \tag{2}$$

with the overdot indicating a time derivative, and

$$L(t) = L_0 - 2U_b t. \tag{3}$$

In the present case, we will work in Cartesian coordinates and take the compressed directions to be along x and y, with the z direction uncompressed. The background flow is such that if we took a cube of initial side length L_0 and put it in the flow, it will have a contracting side length of $L(t)$ along the x and y directions and a constant side length of L_0 in the z direction. The rate of contraction is determined by the compression velocity, U_b.

As in Ref. 8, we will assume homogeneity of the flow under ensemble averaging and ignore density perturbations (low Mach assumption). Consistent with this, the density is spatially constant and increases with compression as expected,

$$\rho(t) = \frac{\rho_0}{\bar{L}^2}, \tag{4}$$

where

$$\bar{L} = \frac{L(t)}{L_0} = 1 - 2\frac{U_b}{L_0}t. \tag{5}$$

Similarly, the temperature, which is determined through the ideal gas equation of state, assuming adiabatic compression, will be spatially uniform, with a time dependence given by $T = T_0\bar{L}^{-4/3}$.

In order to eliminate any explicit spatial dependence from the NS equations, we work in coordinates, $\mathbf{X}$, that move with the background flow, $x = \bar{L}X$, $y = \bar{L}Y$, $z = Z$. Writing $v_i'(\mathbf{x},t) = V_i(\mathbf{X},t)$ and $p'(\mathbf{x},t) = P(\mathbf{X},t)$, the NS momentum equations are

$$\frac{\partial V_x}{\partial t} + \frac{\dot{L}}{L}V_x + \mathrm{C}(V_x) + \frac{\bar{L}}{\rho_0}\frac{\partial P}{\partial X} = \nu_0\bar{\mu}\mathrm{D}(V_x), \tag{6}$$

$$\frac{\partial V_y}{\partial t} + \frac{\dot{L}}{L}V_y + \mathrm{C}(V_y) + \frac{\bar{L}}{\rho_0}\frac{\partial P}{\partial Y} = \nu_0\bar{\mu}\mathrm{D}(V_y), \tag{7}$$

$$\frac{\partial V_z}{\partial t} + \mathrm{C}(V_z) + \frac{\bar{L}^2}{\rho_0}\frac{\partial P}{\partial Z} = \nu_0\bar{\mu}\mathrm{D}(V_z). \tag{8}$$

The continuity equation is

$$\frac{1}{\bar{L}}\left(\frac{\partial V_x}{\partial X} + \frac{\partial V_y}{\partial Y}\right) + \frac{\partial V_z}{\partial Z} = 0. \tag{9}$$

In Eqs. (6)–(8), we have used a shorthand operator form for both the convective term (C) and the viscous dissipation term (D),

$$\mathrm{C}(A) = \frac{1}{\bar{L}}\left(V_x\frac{\partial A}{\partial X} + V_y\frac{\partial A}{\partial Y}\right) + V_z\frac{\partial A}{\partial Z}, \tag{10}$$

$$\mathrm{D}(A) = \frac{\partial^2 A}{\partial X^2} + \frac{\partial^2 A}{\partial Y^2} + \bar{L}^2\frac{\partial^2 A}{\partial Z^2}. \tag{11}$$

The dynamic viscosity, μ, is taken to be $\mu = \mu_0\bar{\mu}(\bar{T})$, with $\bar{T} = T/T_0$. The kinematic viscosity coefficient appearing in Eqs. (6)–(8), ν_0, is $\nu_0 = \mu_0/\rho_0$. For the unmagnetized Braginskii viscosity, we have $\bar{\mu}(\bar{T}) = \bar{T}^{5/2}$.[19] In general, we could consider arbitrary rates of heating (or cooling) during compression and we could also more generally permit ionization effects on the viscosity and study the impacts on the flow compression.[8] A simple first approach to parameterizing these effects is to let $\bar{\mu} = \bar{L}^{-4\beta/3}$, with β being a parameter determined by the net heating and ionization processes in the compression, which are restricted to power-law behavior under compression.[8,11] The simulations in this work will have the adiabatic, ideal gas, 2D compression result for T given above, $\bar{T} = \bar{L}^{-4/3}$, and will assume no ionization. In this case, $\beta = 5/2$ and $\bar{\mu} = \bar{L}^{-10/3}$.

A few features of the 2D compression NS system, Eqs. (6)–(8), stand out. The system is forced (linearly) by the compression in the x and y directions, the second term in Eqs. (6) and (7), while the z direction, Eq. (8), is unforced, and therefore, V_z can only increase in the compression due to nonlinear transfer. The convective term, Eq. (10), has an increasing coefficient on the terms associated with velocities and derivatives in the compression plane (x, y), while the noncompressed direction (z) has a constant coefficient. All velocity components experience viscous dissipation of the same form, Eq. (11). In general, the dissipation due to derivatives along the noncompressed direction (z) is scaled smaller by $\bar{L}^2$ in the compression than derivatives in the compression plane. However, when the viscosity scales as $\bar{\mu} = \bar{L}^{-10/3}$, all viscous terms scale at least as strongly as $\bar{L}^{-4/3}$ in the compression.

III. LINEARIZED BEHAVIOR (VISCOUS RAPID DISTORTION THEORY)

In order to get a basic understanding of the viscous dissipation behavior in the system of NS equations for 2D compression of a variable-viscosity plasma, Eqs. (6)–(9), it is useful to solve the linear system of equations which results from dropping the convective derivative. Both the forcing from the compression and the viscous dissipation are linear in the present model (more generally, with a viscosity that depends on a temperature which is a field, the viscous term will be nonlinear). In an initially rapid compression, the (linear) forcing term will be dominant for the compressed directions at the start of the compression (by definition). If the flow reaches a viscous state, the (linear) viscous term will be dominant. Thus, at least for compressions at a modest Reynolds number, which have an initially rapid phase, and a final viscous phase, we can get some picture of the system behavior with the linear model. Then, also, we will find that the differences between the linear model results and the (nonlinear) simulations can help us understand the essential features of the system. The solution of the system Eqs. (6)–(9), with the convective term dropped, is essentially a viscous version of a rapid distortion theory (RDT) solution.[20]

Our interest is to solve the initial value problem for the system, Eqs. (6)–(9), given an initial incompressible flowfield, $\mathbf{V}(\mathbf{X}, t = 0)$ in

the domain (a cube of side length L_0 in the moving frame) and a compression velocity U_b. We will use periodic boundary conditions. First, we drop the convective derivative, $\mathrm{C}(V_i)$, from Eqs. (6)–(8). Then, we scale the velocity and pressure as

$$V_{x,y} = \bar{L}^{\delta}\tilde{V}_{x,y}, \tag{12}$$

$$V_z = \bar{L}^{\sigma}\tilde{V}_z, \tag{13}$$

$$P = \bar{L}^{\eta}\tilde{P}. \tag{14}$$

Further, we use Eq. (5) to change the time variable to $\bar{L}$, with the compression then proceeding from $\bar{L}=1$ at $t=0$ toward $\bar{L}\to 0$ as $t\to t_f = L_0/2U_b$. Note that because the lab-frame domain collapses to a line at $t=t_f$, we never reach this final time. We select $\sigma=\delta+1$ and $\eta=\delta-1$. These choices allow us to put the momentum equations, Eqs. (6)–(8), on equal footing, including to make each pressure term have identical time scaling. While we can carry through the analysis of this section with general δ, the value will drop out from the final (unscaled) result (as we would hope), and therefore, for convenience, we take $\delta=-1$, which eliminates the compressive forcing from the scaled equation. Then, the scaled momentum equations can be written as

$$\frac{\partial\tilde{V}_i}{\partial\bar{L}} - \frac{t_f}{\rho_0}\frac{\partial\tilde{P}}{\partial X_i} = -\nu_0 t_f \bar{\mu}(\bar{L})\mathrm{D}(\tilde{V}_i), \tag{15}$$

where the index i runs over x, y, z and $X_x=X$, $X_y=Y$, $X_z=Z$. As per the discussion in Sec. II, it is assumed that the viscosity is a function of $\bar{L}$, through the temperature, although we need not specify this function now. After scaling, the continuity equation can be written (for $\bar{L}\neq 0$) as

$$\frac{\partial\tilde{V}_x}{\partial X} + \frac{\partial\tilde{V}_y}{\partial Y} + \bar{L}^2\frac{\partial\tilde{V}_z}{\partial Z} = 0. \tag{16}$$

We now consider the vorticity, $\tilde{\boldsymbol{\omega}} = \nabla\times\tilde{\mathbf{V}}$. Utilizing Eq. (15), we arrive at an equation for the components of $\tilde{\boldsymbol{\omega}}$,

$$\frac{\partial\tilde{\omega}_i}{\partial\bar{L}} = -\nu_0 t_f \bar{\mu}(\bar{L})\mathrm{D}(\tilde{\omega}_i). \tag{17}$$

We will solve the initial value problem of Eq. (17) in Fourier space. Then, we find the Fourier-space velocity expression by inverting the vorticity definition, taking account of the fact that $\tilde{\mathbf{V}}$ satisfies Eq. (16) and is therefore not divergence free except at $\bar{L}=1$ ($t=0$). We define $\tilde{\boldsymbol{\omega}}$ in Fourier space as $\tilde{\boldsymbol{\omega}}(\mathbf{X},t) = \sum_{k_x,k_y,k_z}\hat{\boldsymbol{\omega}}_{\mathbf{k}}(t)\exp(i\mathbf{k}\cdot\mathbf{X})$. Here, the $\mathbf{k}$ values are $k_{x,y,z} = 2\pi n_{x,y,z}/L_0$, with $n_{x,y,z}\in\mathbb{Z}$. The Fourier coefficients are found as usual, $\hat{\boldsymbol{\omega}}_{\mathbf{k}}(t) = \int\int\int \mathrm{d}\mathbf{X}\tilde{\boldsymbol{\omega}}(\mathbf{X},t)\exp(-i\mathbf{k}\cdot\mathbf{X})/L_0^3$, with the integrals taken over the cube of side length L_0. In Fourier space, Eq. (17) is

$$\frac{\mathrm{d}\hat{\boldsymbol{\omega}}_{\mathbf{k}}}{\mathrm{d}\bar{L}} = \nu_0 t_f \bar{\mu}(\bar{L})\left(k_x^2 + k_y^2 + \bar{L}^2 k_z^2\right)\hat{\boldsymbol{\omega}}_{\mathbf{k}}, \tag{18}$$

which can be integrated in $\bar{L}$ in order to find $\hat{\boldsymbol{\omega}}_{\mathbf{k}}(\bar{L})$. Doing so yields

$$\hat{\boldsymbol{\omega}}_{\mathbf{k}}(\bar{L}) = \hat{\boldsymbol{\omega}}_{\mathbf{k},0}\exp\left[\phi(\bar{L},\mathbf{k})\right], \tag{19}$$

$$\phi(\bar{L},\mathbf{k}) = -\nu_0 t_f\int_{\bar{L}}^{1}\bar{\mu}(\bar{L}')\left(k_x^2 + k_y^2 + \bar{L}'^2 k_z^2\right)\mathrm{d}\bar{L}', \tag{20}$$

where the subscript 0 denotes the initial condition, $\hat{\boldsymbol{\omega}}_{\mathbf{k},0} = \hat{\boldsymbol{\omega}}_{\mathbf{k}}(\bar{L}=1)$.

By expressing the curl of the vorticity in terms of second derivatives of the velocity, making use of Eq. (16), and working in Fourier space, we can solve for $\hat{\mathbf{V}}_{\mathbf{k}}$ in terms of $\hat{\boldsymbol{\omega}}_{\mathbf{k}}$. In Fourier space, the curl of the vorticity can be expressed as $-i\mathbf{k}\times\hat{\boldsymbol{\omega}}_{\mathbf{k}} = -(1-\bar{L}^2)\mathbf{k}k_z\hat{V}_{\mathbf{k},z} + \mathbf{k}^2\hat{\mathbf{V}}_{\mathbf{k}}$. First, the z component of this can be solved for $\hat{V}_{\mathbf{k},z}$ (the z component of $\hat{\mathbf{V}}_{\mathbf{k}}$), and then, the x and y components of the velocity can be found. Doing so yields

$$\hat{V}_{\mathbf{k},z} = \hat{V}_{\mathbf{k},z,0}\frac{\mathbf{k}^2}{\mathbf{k}^2 - (1-\bar{L}^2)k_z^2}\exp[\phi], \tag{21}$$

$$\hat{V}_{\mathbf{k},x|y} = \left(\hat{V}_{\mathbf{k},x|y,0} + \hat{V}_{\mathbf{k},z,0}\frac{(1-\bar{L}^2)k_{x|y}k_z}{\mathbf{k}^2 - (1-\bar{L}^2)k_z^2}\right)\exp[\phi], \tag{22}$$

where the subscript $x|y$ indicates either x or y (to be chosen consistently across all such subscripts).

The total energy in the flow $\mathbf{V}$ (integrated over the cubic domain), which is the same as the total energy in the flow $\mathbf{v}'$, can be written as

$$E = \frac{\rho_0 L_0^3}{2}\sum_{k_x,k_y,k_z}\left[\bar{L}^{-2}\left(\hat{V}_{\mathbf{k},x}\hat{V}^*_{\mathbf{k},x} + \hat{V}_{\mathbf{k},y}\hat{V}^*_{\mathbf{k},y}\right) + \hat{V}_{\mathbf{k},z}\hat{V}^*_{\mathbf{k},z}\right]. \tag{23}$$

Here, the asterisk indicates complex conjugation.

Specifying $\bar{\mu} = \bar{L}^{-4\beta/3}$ (see Sec. II), the integral in the exponent ϕ, Eq. (20), can be carried out, yielding

$$\phi = -\frac{2\pi^2}{\mathrm{Re}_U}\left[\frac{1-\bar{L}^{1-4\beta/3}}{1-4\beta/3}\left(n_x^2+n_y^2\right) + \frac{1-\bar{L}^{3-4\beta/3}}{3-4\beta/3}n_z^2\right], \tag{24}$$

where it is assumed $\beta\neq 3/4$, $\beta\neq 9/4$ (separate ϕ expressions valid for these cases can be found). Here, $\mathrm{Re}_U = U_b L_0/\nu_0$ is a Reynolds number using the compression velocity U_b instead of a flow velocity, and n_x, n_y, and n_z are integer mode numbers (from above).

In the case when $\beta = 5/2$ (adiabatic heating of an ideal gas with no ionization), ϕ is

$$\phi = -\frac{2\pi^2}{\mathrm{Re}_U}\left[\frac{3}{7}\left(\bar{L}^{-7/3}-1\right)\left(n_x^2+n_y^2\right) + 3\left(\bar{L}^{-1/3}-1\right)n_z^2\right]. \tag{25}$$

IV. DISCUSSION AND COMPARISON WITH SIMULATIONS

We now discuss the behavior of the 2D compression system, Eqs. (6)–(9), as it relates to viscous dissipation. First, we focus our analysis on the linear (viscous RDT) solution given in Sec. III. Then, we compare the linear solution with direct numerical simulations (DNSs) of the 2D compression system carried out in the pseudospectral code Dedalus,[21,22] which, among other things, will show the important influence of nonlinear transfer to larger scales on the viscous dissipation process (or lack thereof).

The energy behavior of the linear (viscous RDT) solution to the 2D compression of 3D flow is given by Eq. (23), evaluated with Eqs. (21), (22), and, most generally, with ϕ given by Eq. (20). Broadly, examining Eq. (20) [or Eqs. (24) and (25)], we see that there are two classes of Fourier modes in terms of their viscous damping behavior.

First, there are modes with $k_x \neq 0$ and/or $k_y \neq 0$. For these modes, the dominant viscous damping contribution as $\bar{L} \to 0$ will come from the nonzero k_x or k_y component (derivatives in the plane of compression). Second, there are modes for which $k_x = k_y = 0$. For these modes, only the k_z component of ϕ contributes to damping; since the exponent for these modes is scaled smaller by $\bar{L}^2$, these modes will be much more resistant to viscous damping than modes with either (or both) $k_x \neq 0$ or $k_y \neq 0$, for a given $|\mathbf{k}|$.

This distinction between the two mode classes should become apparent in the case when the viscosity increases sufficiently in the compression (such that the value of the viscosity has an influence on the flow). Parameterizing the net heating and ionization influence with β, as discussed in Sec. II, and therefore also the rate of viscosity increase (or decrease) in compression ($\bar{\mu} = \bar{L}^{-4\beta/3}$), we have ϕ as given by Eq. (24). When $\beta > 9/4$, all Fourier modes are exponentially damped in the linear model, which, after sufficient compression, will overcome the $\bar{L}^{-2}$ scaling in the energy, Eq. (23), such that eventually all Fourier modes will be damped, linearly. Thus, in this case, the energy should eventually viscously dissipate under continuing compression. Since $\beta = 5/2$ for an adiabatic compression of an ideal gas, with no ionization, this situation falls into the $\beta > 9/4$ case presently discussed. The simulations in this work focus on the $\beta = 5/2$ situation, and as such, most of our discussion will as well. Before specializing to the $\beta = 5/2$ situation, we finish considering the impact of the two broad linear mode classes for other values of β.

When $3/4 < \beta < 9/4$, all modes in the first mode class ($k_{x|y} \neq 0$) are still damped linearly after sufficient compression, while this will no longer be the case for the second mode class ($k_x = k_y = 0$); for the latter class, the mode growth due to the compression can outpace the viscous damping as $\bar{L} \to 0$, in the linear solution. Then, we expect that the system will have a tendency to pile energy in modes with $k_x = k_y = 0$ and that the efficiency (or inefficiency) of nonlinear exchange from these modes into modes with $k_{x|y} \neq 0$ may be important in setting the system behavior under continuing compression. Nonlinear transfer to $k_x = k_y = 0$ modes with higher k_z may also be important in setting the system behavior. When $\beta < 3/4$, no modes at a fixed $|\mathbf{k}|$ are damped linearly as $\bar{L} \to 0$, and both cascade to higher mode numbers and transfer between mode classes may be important. These problems are beyond the scope of the current work, and we now focus on the viscous dissipation behavior of the $\beta = 5/2$ case and a surprising influence of the nonlinearity in this case.

When $\beta = 5/2$, the exponent ϕ in the linear solution, Eqs. (21)–(22), is given by Eq. (25). In Fig. 1, the red solid line shows the linear turbulent kinetic energy (TKE) solution, Eq. (23) vs compression ratio ($\bar{L}$) for $\beta = 5/2$ and $\mathrm{Re}_U = 375$. The initial condition is a saturated, isotropic, turbulent state with 128 Fourier modes in each direction (128^3 total modes), generated by using Dedalus to solve the Navier-Stokes equations with the real-space forcing scheme described by Lundgren[23] (see also Rosales and Meneveau[24]). We use a box of side length $L_0 = 1$, with $\nu = 1/600$ and $A = 1.45$, in the notation of Rosales and Meneveau.[24] The numerical pseudospectral solution uses 196^3 modes dealiased to 128^3. This particular initial condition has a Taylor Reynolds number $\mathrm{Re}_\lambda \approx 101$, a mean initial kinetic energy $E_0 = \langle \mathbf{V}^2/2 \rangle \approx 0.87$, and an initial mean viscous dissipation $\epsilon_0 = -\nu \langle \mathbf{V} \cdot \nabla^2 \mathbf{V} \rangle \approx 2.6$. The energy spectrum of the initial condition is in line with those typically generated by the real-space forcing scheme, see, e.g., Figs. 11 and 12 in Rosales and Meneveau.[24] Of particular note is that this initial condition contains all modes (except $k_x = k_y = k_z = 0$). While not a general feature, for this particular Re_U and initial condition, we can see in Fig. 1 that the energy experiences two growth phases (increasing energy as $\bar{L}$ decreases) as the compression progresses, each followed by a dissipation phase where the energy decreases. These two dissipation phases, which are well-separated in compression ratio $\bar{L}$, correspond to first modes with $k_{x|y} \neq 0$ dissipating, followed much later by modes with $k_x = k_y = 0$ dissipating.

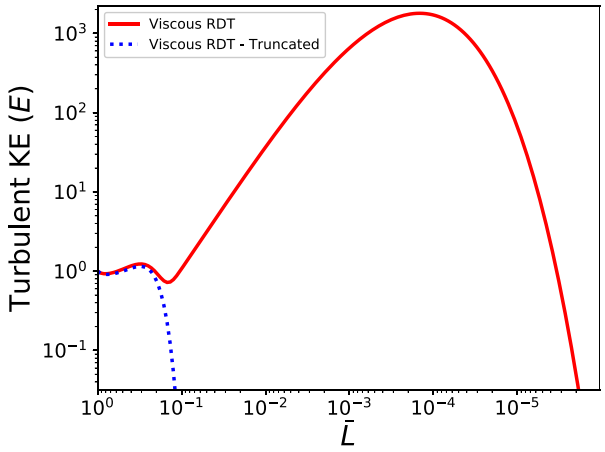

FIG. 1. The evolution of the turbulent kinetic energy (TKE) as a function of (linear) compression ratio for two different initial conditions for a two-dimensional, constant velocity compression of an initially isotropic turbulent flowfield. The TKE evolves according to the linear viscous rapid distortion theory (RDT) solution, Eq. (23), with Eqs. (21), (22), and (25). The red solid line shows two growth phases (increasing TKE with decreasing $\bar{L}$), each followed by a dissipation phase, corresponding to a different class of Fourier mode being dissipated. First modes with variation in the compression plane dissipate ($k_{x|y} \neq 0$), and then, after much more compression, modes with variation only in the noncompressed direction dissipate ($k_x = k_y = 0$). This point is emphasized by the dashed blue line, which uses the same initial condition, but with $k_x = k_y = 0$ modes removed. In addition to emphasizing the difference in mode behavior, this could also correspond to the linear behavior in a situation where such modes ($k_x = k_y = 0$) are disallowed, for example, by hard-wall boundary conditions. In both cases, the initial energy is normalized to 1, $\beta = 5/2$, and $\mathrm{Re}_U = 375$, see Sec. IV for more discussion.

To further illustrate the substantial difference in the dissipation characteristics of the two mode classes, we can "truncate" the spectrum of Fourier modes in the initial condition. In this work, we truncate the initial condition by zeroing out the energy in all modes with $k_x = k_y = 0$; that is, we remove all initial energy from the second mode class. The blue dashed line in Fig. 1 shows the linear energy solution, Eq. (23), with this truncated linear spectrum, again for $\beta = 5/2$ and $\mathrm{Re}_U = 375$. In this case, we see that the initial energy behavior is similar (albeit with somewhat lower energy growth in the first growth phase) but that the first dissipation phase completely dissipates the energy, with the energy then remaining at 0 for the rest of the compression. This further illustrates that the first dissipation phase noted in the full-spectrum case (red solid line) is in fact due to the $k_{x|y} \neq 0$ modes dissipating.

We now consider the energy behavior of the full (nonlinear) system, Eqs. (6)–(9), and again the situation where the viscous behavior is adiabatic, no ionization, $\beta = 5/2$. We use Dedalus to simulate the

nonlinear evolution of the same two initial conditions (full and truncated) that were used to calculate to the viscous RDT solution for Fig. 1. We set $\nu_0 = 1/600$ and use $L_0 = \rho_0 = 1$. The compression velocity is set such that the initial compression time, $\tau_{c,0} = L_0/2U_b$, is 1/10 the initial turbulent dissipation time scale, $\tau_{t,0} = E_0/\epsilon_0$. For the untruncated spectrum, this corresponds to $U_b \approx 15$, while the required velocity for the truncated spectrum is slightly different, $U_b \approx 16$ (in the truncated case, $E_0 \approx 0.75$ and $\epsilon_0 \approx 2.5$). Thus, in both cases, we have an initially "fast" compression (by a factor of 10), and we expect the TKE to initially grow; this is in fact the case, as seen in Fig. 2, with the TKE in the full-spectrum case plotted as the solid blue line and the energy in the truncated-spectrum case plotted as the dotted green line. After this initial growth under compression, the TKE in each case behaves in a qualitatively similar fashion to the corresponding case of the linear RDT solution, with one particularly notable difference. In Fig. 2, we see that the truncated spectrum TKE no longer dissipates to 0 in the initial dissipation of $k_{x|y} \neq 0$ modes (instead reaching a minimum energy in this case similar to the initial energy). Even though this case starts with zero energy in $k_x = k_y = 0$ modes, the nonlinearity has transferred some energy into these modes before the $k_{x|y} \neq 0$ mode energy dissipates. If we continue the compression further, the TKE in the nonlinear, truncated-spectrum case will grow up very substantially after the initial dissipation phase. This is in contrast to the linear case, where the lack of initial energy in the $k_x = k_y = 0$ modes persists and the energy dissipates for good in the initial dissipation.

Note that we have used a much lower value of Re_U in the linear viscous RDT cases in Fig. 1 compared to the nonlinear simulations in

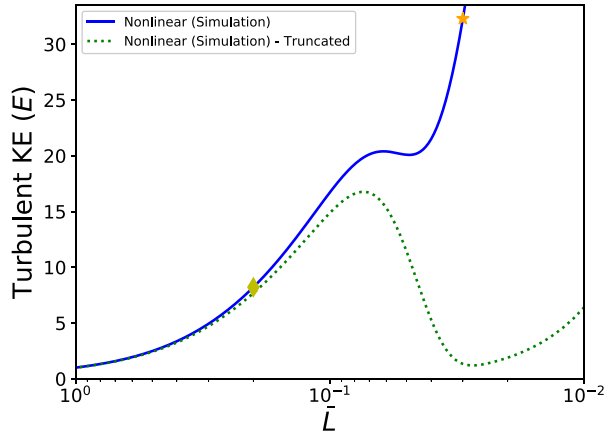

FIG. 2. Similar to Fig. 1, but now with the TKE evolution given by the numerical solution to the full (nonlinear) equations for 2D compression, Eqs. (6)–(9). The same compression of an isotropic, turbulent, initial condition is carried out, with the difference between the two cases shown being that the dashed green line shows the TKE evolution when the initial condition has all energy in $k_x = k_y = 0$ modes removed ("truncated"). However, now, unlike in the linear case shown in Fig. 1, the nonlinearity transfers energy into $k_x = k_y = 0$ modes during the compression of the truncated case; as a result, the energy in this case no longer fully dissipates and begins to grow again after the dissipation of $k_{x|y} \neq 0$ modes. Thus, unless $k_x = k_y = 0$ modes are forbidden, say, by hard-wall boundary conditions, it will be difficult to dissipate the TKE through viscosity, even in this case with a modest initial viscosity ($\nu_0 = 1/600$) and strong viscous growth during compression ($\beta = 5/2$). The cases shown use a compression velocity such that the initial compression rate is 10 times the initial turbulent dissipation time, see Sec. IV for more discussion.

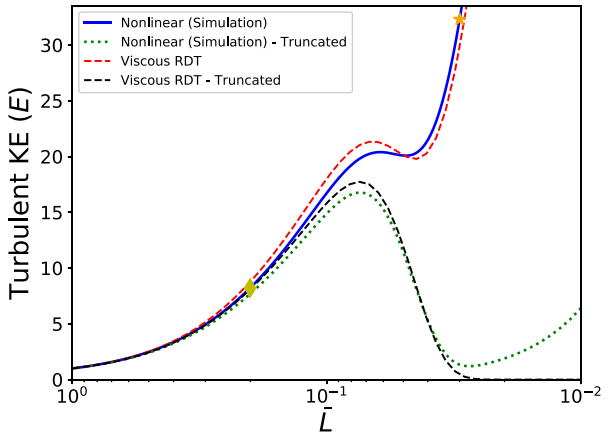

FIG. 3. The same as Fig. 2, but also showing, for comparison, the nontruncated viscous RDT solution (red dashed) and the truncated viscous RDT solution (black - dashed) associated with each nonlinear simulation. Prior to the dissipation of the $k_{x|y} \neq 0$ modes, the RDT solution overpredicts the TKE, because, on the net, the nonlinearity cascades energy to the dissipation scale, leading to more dissipation than the linear case. However, after the dissipation of the $k_{x|y} \neq 0$ modes, the RDT solution underpredicts the TKE, because it has not accounted for nonlinear transfer into $k_x = k_y = 0$ modes.

Fig. 2, in order to more easily reach the point of the second dissipation, which already occurs only after a huge compression ratio for this modest value of Re_U. Figure 3 shows a comparison of the nonlinear simulation results in Fig. 2 with the viscous RDT solution.

In order to give a visual sense of the flow during the compression, we plot slices (y, z) through the domain, at $x = \bar{L}/2$, both early ($\bar{L} = 0.2$, before the domination by $k_x = k_y = 0$ modes) and late ($\bar{L} = 0.03$, after the domination by $k_x = k_y = 0$ modes), in the compression, in Figs. 4 and 5, respectively. The corresponding locations in the TKE behavior figure, Fig. 2, are indicated by a yellow diamond ($\bar{L} = 0.2$, Fig. 4) and by an orange star ($\bar{L} = 0.03$, Fig. 5). Note that in both Figs. 4 and 5, each flow-field plot is stretched in y (has a wrong aspect ratio), in order to make the plots readable. We can see in Fig. 5 that where the flow is dominated by $k_x = k_y = 0$ modes, it correspondingly has structure almost exclusively in the z direction (plots in the x, y plane are nearly constant). Since this direction is uncompressed, the viscous derivatives act more weakly and allow the preservation of this structure. Note also that V_x and V_y velocity magnitudes are much larger than the V_z velocity magnitude (which appears $\sim$0 when plotted on the same scale as the x and y components). This is reflective of the fact that, in this case, the nonlinearity has been ineffective at transferring energy from the linearly forced x and y directions into the linearly unforced z direction. This fact is already apparent in Fig. 4, where we observe that the V_z velocities are smaller than the V_x or V_y velocities; the initial condition is isotropic.

V. CONCLUSION AND IMPLICATIONS

In summary, we show that two "classes" of Fourier modes are important in determining the viscous dissipation behavior of 3D flows compressed in 2D. In Cartesian coordinates, these two classes are first modes with $k_{x|y} \neq 0$ and second modes with $k_x = k_y = 0$, but we may expect that these classes will translate to alternate coordinate

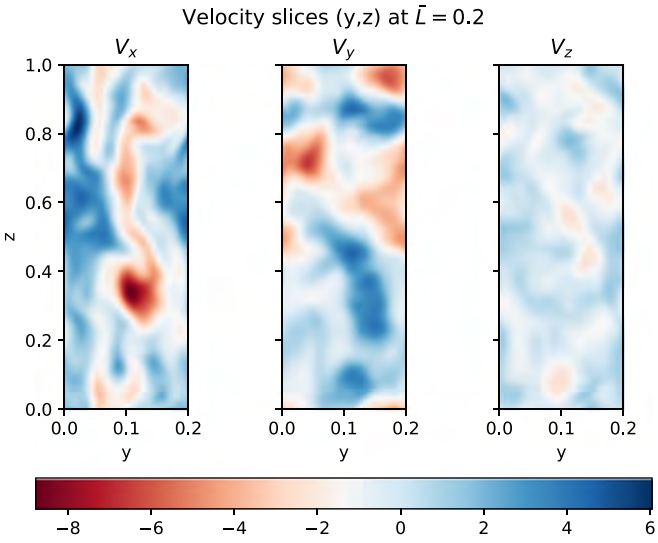

FIG. 4. Slices through the midplane ($x = 0.5\bar{L}$) of the simulation domain at $\bar{L} = 0.2$ showing the velocity components partway through the compression for the nonlinear simulation in solid blue in Fig. 2. This point in the compression is indicated by the yellow diamond in that figure. The velocity field slices show the structure in both the y and z directions; the structure in the y direction is reflective of the presence of $k_y \neq 0$ modes, which have not yet dissipated in the dissipation phase observable in Fig. 2. The magnitude of V_z is smaller than the magnitude of the other velocity components; apparently, the nonlinearity is not sufficient in this case to isotropize the linearly forced components (V_x, V_y) with the linearly unforced V_z component. See Sec. IV. Note that the y direction is "stretched" for readability of the slices; the aspect ratio is not 5 : 1 in $L_z : L_y$ as would be indicated by $\bar{L} = 0.2$.

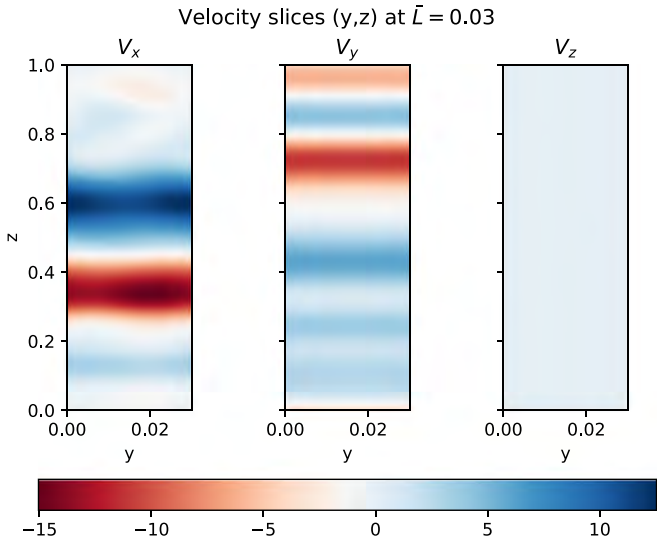

FIG. 5. Slices through the midplane ($x = 0.5\bar{L}$) of the simulation domain at $\bar{L} = 0.03$ showing the velocity components partway through the compression for the nonlinear simulation in solid blue in Fig. 2. This point in the compression is indicated by the orange star in that figure. Unlike the velocity field slices in Fig. 4, the field now has a structure almost exclusively in the z direction; this is reflective of the fact that the viscosity has dissipated most of the energy in $k_y \neq 0$ modes, with energy primarily remaining in $k_x = k_y = 0$ modes. Continuing the trend observable in Fig. 4, the magnitude of V_z is now relatively even smaller than the magnitude of the other velocity components; on this uniform scale, no structure is visible (but there is an observable structure if plotted on a velocity scale with a smaller magnitude). As shown in Fig. 4, the slices are "stretched" in the y direction for the sake of readability.

systems; for example, in cylindrical coordinates, the coordinate pair x, y should be translatable into the coordinate pair r, θ.

The second class of modes, $k_x = k_y = 0$, is much more difficult to dissipate viscously, due to the fact that all the structures are in the z direction which is uncompressed and therefore has a length scale that does not enhance derivatives through shrinking. Furthermore, even if this class of modes is not present in the flow at the start of the compression, the nonlinearity can transfer energy into it, thereby greatly increasing the difficulty of fully dissipating the initial nonradial flow through increasing viscosity from temperature growth in compression. Even in the example cases here, with rapid initial compression of modest initial Reynolds numbers (~600) and perfect adiabatic heating increasing the unmagnetized Braginskii viscosity, we find extreme compression ratios ($L/L_0 \gg 10^{-2}$) are needed to induce dissipation when all modes are present (blue solid line in Fig. 2). One could reduce the required amount of compression to achieve viscous dissipation of the difficult-to-dissipate modes by any of the following: less rapid compression, higher initial viscosity, or a faster rate of heating (viscosity rise) with compression than the adiabatic heating due solely to compression considered here.

While the nonlinearity, by being able to transfer energy into modes with $k_x = k_y = 0$, can make completely dissipating the TKE through viscosity difficult, we can see, from the green dashed line in Fig. 2, that, at least temporarily, we may dissipate much of the TKE through compression, at least when we start with no energy in such modes. The presence or absence of these modes will likely be influenced by a number of factors, including any instabilities present in the system, as well as boundary conditions. For example, hard-wall boundary conditions in the compression directions (x and y here) will disallow modes with $k_x = k_y = 0$, thereby meaning the TKE should completely dissipate with the dissipation of the first class of modes ($k_{x|y} \neq 0$, in this case, both k_x and k_y being nonzero).

There are three contexts in which we briefly consider the implications of the present work.

The first is the proposed utilization of viscous dissipation in a scheme for achieving fusion or a burst of X-rays,[7] which has previously been investigated in 3D compressions. We note first that this scheme imagines supersonic nonradial flows, where the TKE dominates the thermal energy, and the feedback of dissipated TKE into thermal energy has an important influence on the temperature and therefore also on the viscosity and the dissipation process. Therefore, we should be cautious in using the present results to consider the scheme; nonetheless, if modes in the second mode class ($k_x = k_y = 0$) are not forbidden for some reason and are present from early in the compression, we expect it to be difficult to trigger viscous dissipation in light of the results here. If these modes are forbidden or if there is essentially no energy in them from the start of the compression, the scheme may still have promise in the 2D compression case. Also, if the rate of heating during the compression (or at its conclusion) is greater than that considered here (so that $\beta > 5/2$), it will be easier to achieve viscous dissipation, due to the sensitivity of the viscosity to the temperature. Such heating could be provided by the release of dissipated TKE

into thermal energy when the TKE is substantial or through other effects, such as in fast ignition mechanisms instigated by beams or lasers.

The second is in relation to gas-puff Z-pinch experiments (which are 2D plasma compressions) that have inferred large quantities of nonradial hydrodynamic motion,[25] which apparently persists at stagnation as TKE.[25,26] The plasma in these experiments remains inviscid throughout the compression and stagnation; indeed, if the plasma was viscous enough to reach a state like that in Fig. 5, measurements made along radial lines of sight may not infer TKE, since the plasma motion is approximately uniform along any given x, y plane. This of course will depend on the z extent of plasma that is averaged over in the measurement, and we should be cautious in applying the present results to these gas-puff Z-pinch experiments, both because the flows there are supersonic and because while the magnetic field pressure is a very small contribution at stagnation,[26–28] its potential influence must still be examined.

The third context in which we consider the implications of the present work is the generally expected flow state of the deuterium-tritium (D-T) fuel in inertial fusion experiments which utilize 2D compression. In particular, it is suggested that viscous effects can substantially influence the flow field in the high-temperature D-T fuel late (near bang time) in 3D inertial fusion experiments.[5,6] Fusion schemes utilizing 2D compression, such as the magnetoinertial-fusion concept MagLIF,[3,4] may also reach a viscous flow regime near bang-time; this is because they aim to reach similarly high temperatures in D-T fuel and have a similar linear length scale in the compression directions and characteristic compression (flow) velocities which are not larger than the 3D cases. However, to the extent that it applies, the present work hints that it may be difficult in such 2D compressions to dissipate uniform flows in the compression plane with slow variation along the uncompressed direction z, that is, flows with a structure similar to those in Fig. 5. Of course, the present work does not include any magnetic field, nor is it clear what the appropriate effective fuel boundary conditions are for an experiment such as MagLIF. The influence of a strong applied magnetic field could substantially change the results, and this case should be considered in future work. Nonetheless, we hope the present work serves as a useful starting point for considering viscous dissipation in 2D compressions.

ACKNOWLEDGMENTS

This work was supported in part by research Grant Nos. NNSA 67350-9960 (Prime No. DOE DE-NA0001836) and NSF Contract No. PHY-1506122. One of us (S.D.) was supported by the U.S. Department of Energy Fusion Energy Sciences Postdoctoral Research Program administered by the Oak Ridge Institute for Science and Education (ORISE) for the DOE. ORISE is managed by Oak Ridge Associated Universities (ORAU) under DOE Contract No. DE-SC0014664.

REFERENCES

[1]E. I. Moses, R. N. Boyd, B. A. Remington, C. J. Keane, and R. Al-Ayat, Phys. Plasmas **16**, 041006 (2009).
[2]M. J. Edwards, P. K. Patel, J. D. Lindl, L. J. Atherton, S. H. Glenzer, S. W. Haan, J. D. Kilkenny, O. L. Landen, E. I. Moses, A. Nikroo, R. Petrasso, T. C. Sangster, P. T. Springer, S. Batha, R. Benedetti, L. Bernstein, R. Betti, D. L. Bleuel, T. R. Boehly, D. K. Bradley, J. A. Caggiano, D. A. Callahan, P. M. Celliers, C. J. Cerjan, K. C. Chen, D. S. Clark, G. W. Collins, E. L. Dewald, L. Divol, S. Dixit, T. Doeppner, D. H. Edgell, J. E. Fair, M. Farrell, R. J. Fortner, J. Frenje, M. G. Gatu Johnson, E. Giraldez, V. Y. Glebov, G. Grim, B. A. Hammel, A. V. Hamza, D. R. Harding, S. P. Hatchett, N. Hein, H. W. Herrmann, D. Hicks, D. E. Hinkel, M. Hoppe, W. W. Hsing, N. Izumi, B. Jacoby, O. S. Jones, D. Kalantar, R. Kauffman, J. L. Kline, J. P. Knauer, J. A. Koch, B. J. Kozioziemski, G. Kyrala, K. N. LaFortune, S. L. Pape, R. J. Leeper, R. Lerche, T. Ma, B. J. MacGowan, A. J. MacKinnon, A. Macphee, E. R. Mapoles, M. M. Marinak, M. Mauldin, P. W. McKenty, M. Meezan, P. A. Michel, J. Milovich, J. D. Moody, M. Moran, D. H. Munro, C. L. Olson, K. Opachich, A. E. Pak, T. Parham, H.-S. Park, J. E. Ralph, S. P. Regan, B. Remington, H. Rinderknecht, H. F. Robey, M. Rosen, S. Ross, J. D. Salmonson, J. Sater, D. H. Schneider, F. H. Sguin, S. M. Sepke, D. A. Shaughnessy, V. A. Smalyuk, B. K. Spears, C. Stoeckl, W. Stoeffl, L. Suter, C. A. Thomas, R. Tommasini, R. P. Town, S. V. Weber, P. J. Wegner, K. Widman, M. Wilke, D. C. Wilson, C. B. Yeamans, and A. Zylstra, Phys. Plasmas **20**, 070501 (2013).
[3]S. A. Slutz, M. C. Herrmann, R. A. Vesey, A. B. Sefkow, D. B. Sinars, D. C. Rovang, K. J. Peterson, and M. E. Cuneo, Phys. Plasmas **17**, 056303 (2010).
[4]S. A. Slutz and R. A. Vesey, Phys. Rev. Lett. **108**, 025003 (2012).
[5]C. R. Weber, D. S. Clark, A. W. Cook, L. E. Busby, and H. F. Robey, Phys. Rev. E **89**, 053106 (2014).
[6]D. S. Clark, M. M. Marinak, C. R. Weber, D. C. Eder, S. W. Haan, B. A. Hammel, D. E. Hinkel, O. S. Jones, J. L. Milovich, P. K. Patel, H. F. Robey, J. D. Salmonson, S. M. Sepke, and C. A. Thomas, Phys. Plasmas **22**, 022703 (2015).
[7]S. Davidovits and N. J. Fisch, Phys. Rev. Lett. **116**, 105004 (2016).
[8]S. Davidovits and N. J. Fisch, Phys. Rev. E **94**, 053206 (2016).
[9]S. Davidovits and N. J. Fisch, Phys. Plasmas **24**, 122311 (2017).
[10]G. Viciconte, B.-J. Gréa, and F. S. Godeferd, Phys. Rev. E **97**, 023201 (2018).
[11]S. Davidovits and N. J. Fisch, Phys. Plasmas **25**, 042703 (2018).
[12]A. Campos and B. E. Morgan, Phys. Rev. E **99**, 013107 (2019).
[13]A. Campos and B. E. Morgan, Phys. Rev. E **99**(6), 063103 (2019).
[14]S. Davidovits and N. J. Fisch, Phys. Plasmas **26**(6), 062709 (2019).
[15]B. A. Hammel, H. A. Scott, S. P. Regan, C. Cerjan, D. S. Clark, M. J. Edwards, R. Epstein, S. H. Glenzer, S. W. Haan, N. Izumi, J. A. Koch, G. A. Kyrala, O. L. Landen, S. H. Langer, K. Peterson, V. A. Smalyuk, L. J. Suter, and D. C. Wilson, Phys. Plasmas **18**, 056310 (2011).
[16]S. P. Regan, R. Epstein, B. A. Hammel, L. J. Suter, J. Ralph, H. Scott, M. A. Barrios, D. K. Bradley, D. A. Callahan, C. Cerjan, G. W. Collins, S. N. Dixit, T. Doeppner, M. J. Edwards, D. R. Farley, S. Glenn, S. H. Glenzer, I. E. Golovkin, S. W. Haan, A. Hamza, D. G. Hicks, N. Izumi, J. D. Kilkenny, J. L. Kline, G. A. Kyrala, O. L. Landen, T. Ma, J. J. MacFarlane, R. C. Mancini, R. L. McCrory, N. B. Meezan, D. D. Meyerhofer, A. Nikroo, K. J. Peterson, T. C. Sangster, P. Springer, and R. P. J. Town, Phys. Plasmas **19**, 056307 (2012).
[17]T. Ma, P. K. Patel, N. Izumi, P. T. Springer, M. H. Key, L. J. Atherton, L. R. Benedetti, D. K. Bradley, D. A. Callahan, P. M. Celliers, C. J. Cerjan, D. S. Clark, E. L. Dewald, S. N. Dixit, T. Döppner, D. H. Edgell, R. Epstein, S. Glenn, G. Grim, S. W. Haan, B. A. Hammel, D. Hicks, W. W. Hsing, O. S. Jones, S. F. Khan, J. D. Kilkenny, J. L. Kline, G. A. Kyrala, O. L. Landen, S. Le Pape, B. J. MacGowan, A. J. Mackinnon, A. G. MacPhee, N. B. Meezan, J. D. Moody, A. Pak, T. Parham, H.-S. Park, J. E. Ralph, S. P. Regan, B. A. Remington, H. F. Robey, J. S. Ross, B. K. Spears, V. Smalyuk, L. J. Suter, R. Tommasini, R. P. Town, S. V. Weber, J. D. Lindl, M. J. Edwards, S. H. Glenzer, and E. I. Moses, Phys. Rev. Lett. **111**, 085004 (2013).
[18]B. M. Haines, G. P. Grim, J. R. Fincke, R. C. Shah, C. J. Forrest, K. Silverstein, F. J. Marshall, M. Boswell, M. M. Fowler, R. A. Gore, A. C. Hayes-Sterbenz, G. Jungman, A. Klein, R. S. Rundberg, M. J. Steinkamp, and J. B. Wilhelmy, Phys. Plasmas **23**, 072709 (2016).
[19]S. I. Braginskii, Rev. Plasma Phys. **1**, 205 (1965), see https://ui.adsabs.harvard.edu/abs/1965RvPP....1..205B.
[20]J. C. R. Hunt and D. J. Carruthers, J. Fluid Mech. **212**, 497 (1990).
[21]See http://dedalus-project.org for code source, documentation, and developer information.

[22]K. J. Burns, G. M. Vasil, J. S. Oishi, D. Lecoanet, and B. Brown, "Dedalus: Flexible framework for spectrally solving differential equations," Astrophys. Source Code Library, arXiv:1905.10388 (2019).
[23]T. S. Lundgren, *Annual Research Briefs* (Center for Turbulence Research, Stanford, 2003), pp. 461–473.
[24]C. Rosales and C. Meneveau, Phys. Fluids **17**, 095106 (2005).
[25]E. Kroupp, D. Osin, A. Starobinets, V. Fisher, V. Bernshtam, L. Weingarten, Y. Maron, I. Uschmann, E. Förster, A. Fisher, M. E. Cuneo, C. Deeney, and J. L. Giuliani, Phys. Rev. Lett. **107**, 105001 (2011).
[26]E. Kroupp, E. Stambulchik, A. Starobinets, D. Osin, V. I. Fisher, D. Alumot, Y. Maron, S. Davidovits, N. J. Fisch, and A. Fruchtman, Phys. Rev. E **97**, 013202 (2018).
[27]Y. Maron, A. Starobinets, V. I. Fisher, E. Kroupp, D. Osin, A. Fisher, C. Deeney, C. A. Coverdale, P. D. Lepell, E. P. Yu, C. Jennings, M. E. Cuneo, M. C. Herrmann, J. L. Porter, T. A. Mehlhorn, and J. P. Apruzese, Phys. Rev. Lett. **111**, 035001 (2013).
[28]G. Rosenzweig, E. Kroupp, A. Starobinets, A. Fisher, and Y. Maron, in 2014 IEEE 41st International Conference on Plasma Sciences (ICOPS) (2014), pp. 1–1.